Check for updates

Received: 9 November 2023 | Revised: 26 January 2024 | Accepted: 3 March 2024

DOI: 10.1002/pen.26704

RESEARCH ARTICLE

POLYMER ENGINEERING AND SCIENCE WILEY

Effects of carbon-based nanoparticles on the properties of poly(lactic acid) hybrid composites containing basalt fibers and carbon-based nanoparticles processed by injection molding

Zsolt Juhász[1] | **Balázs Pinke**[1] | **Bence Gonda**[1] | **László Mészáros**[1,2]

[1]Department of Polymer Engineering, Faculty of Mechanical Engineering, Budapest University of Technology and Economics, Budapest, Hungary

[2]HUN-REN-BME Research Group for Composite Science and Technology, Budapest, Hungary

Correspondence
László Mészáros, Department of Polymer Engineering, Faculty of Mechanical Engineering, Budapest University of Technology and Economics, Műegyetem rkp. 3., H-1111 Budapest, Hungary.
Email: meszaros@pt.bme.hu

Funding information
Magyar Tudományos Akadémia; Nemzeti Kutatási, Fejlesztési és Innovációs Alap, Grant/Award Numbers: TKP2021-NVA, ÚNKP-23-5-BME-434

Abstract

In this study, we developed composites with a poly(lactic acid) matrix and reinforced with basalt fiber, carbon-based nanoparticles (carbon nanotube [CNT] and expanded graphene [GNP]), and both basalt fiber and nanoparticles (hybrid composites). The composites were produced by extrusion, and then tensile specimens were injection molded from the composites. The hybrid composites exhibited enhanced mechanical properties. The reinforcing materials increased crystallinity; this was more pronounced for hybrid composites. We experienced significant increase in the glass transition temperature, which proves the better interaction between the reinforcing and the matrix phases. Dynamic mechanical thermal analysis showed that the nanoparticles increased the storage modulus both alone and in combination with basalt fibers. Furthermore, the basalt fiber-reinforced composites and hybrids exhibited significant modulus above the glass transition temperature. Based on scanning electron microscopy images of the fracture surfaces, we concluded that adding basalt fibers during compounding resulted in better dispersion of the nanoparticles.

Highlights

- Poly(lactic acid) (PLA) reinforced with basalt fiber has good strength properties.
- Graphene hybrid exhibits notable tensile modulus improvement in hybrids.
- Graphene and carbon nanotubes are crystalline nucleating agents for PLA.
- Enhanced nanoparticle distribution was discovered for hybrid composites.
- The glass transition temperature of PLA increases with reinforcement.

KEYWORDS

basalt fiber, carbon nanotube, graphene, hybrid composites, poly(lactic acid)

This is an open access article under the terms of the Creative Commons Attribution License, which permits use, distribution and reproduction in any medium, provided the original work is properly cited.
© 2024 The Authors. *Polymer Engineering & Science* published by Wiley Periodicals LLC on behalf of Society of Plastics Engineers.

1 | INTRODUCTION

Plastic waste is an important issue globally, encouraging more and more people and companies to use environmentally friendly materials. Therefore, many research groups focus on bio-based materials for different applications.[1–4] A promising candidate is poly(lactic acid) (PLA), which is a much researched biodegradable, renewable resource-based polymer. PLA is a thermoplastic, aliphatic polyester mainly produced from L-lactic acid monomer, which can be synthesized from glucose, through polycondensation, or the ring-opening polymerization of L-lactide rings mainly. In polylactic acid produced from renewable resources, there is also a D-isomer in addition to the L-isomer. The ratio of these two isomers affects the tendency of the polymer to crystallize. Therefore, there are amorphous and semi-crystalline PLAs. However, it is difficult to produce significant crystallinity even in PLAs that tend to crystallize. A high crystalline ratio can be obtained by cooling PLA slowly from the melt (<1°C/min) or with nucleating agents. The mechanical properties of PLA are similar to some petroleum-based commodity plastics, such as polyethylene terephthalate (PET) or polystyrene (PS), but it also depends on the type of PLA (amorphous or semi-crystalline). Its tensile strength is 60–65 MPa, and its tensile modulus is around 3 GPa. PLA is a rigid material with an elongation at break of only 2%–5%. However, plasticizers can improve its flexibility.[5–14]

Unfortunately, PLA often does not have suitable properties to be used as a structural material, but with reinforcement and additives, its mechanical properties can be greatly improved and it can be made suitable for engineering applications.[15] One promising reinforcing material is basalt fiber. It has good mechanical properties (e.g., strength, tensile modulus, and high elongation at break), and outstanding chemical, thermal, and weather resistance. It is also a good sound insulator and an excellent electrical insulator. These attributes, its relatively low price, and its good thermal stability make basalt fiber a competitive reinforcing material (similar to glass fiber).[16,17]

Besides the generally applied micro-sized reinforcements, well-dispersed nanosized materials have a good complementary effect on the properties of composites.[18] Carbon-based materials are often used for nanosized reinforcement. The two most extensively studied allotropes of carbon are carbon nanotubes (CNTs) and graphene, due to their high flexibility, large specific surface, low density, and superior electrical, thermal, and mechanical properties. However, one of the most significant disadvantages of reinforcing nanomaterials is that they are difficult to disperse homogeneously in the material, and therefore their positive effects often cannot be fully exploited.[19] Our previous studies indicate that commingling with microparticles may solve this problem, as they improve the dispersion of the nanoparticles.[20,21]

In many cases, synergistic effects were found that resulted in improved properties. For instance, hybrid composites with properly chosen combination of nano- and microsized fillers can produce significantly higher electrical conductivity than each material used separately.[22] We also saw this synergistic effect in our hybrid composite (PLA reinforced with carbon fibers and CNTs).[23] In some cases, nanoparticles can be used to improve the adhesion between the matrix and the micro-sized reinforcing material.[24,25] In general, nanomaterials positively affect the thermal (stability, thermal conductivity) and mechanical properties of common composites.[26–28]

Overall, with the right additives and reinforcing materials, the properties of PLA can be optimized for engineering applications, thus it can be used outside the packaging industry as well. In this study, we prepared and investigated nanocomposites with a PLA matrix and graphene or CNTs, and the hybridization effect of basalt fiber.

2 | EXPERIMENTAL

2.1 | Materials

NatureWorks LLC (Minnetonka, USA) supplied the PLA (IngeoTM 8052D). The micro-sized reinforcement material was KV02 basalt fiber (BF) with an average diameter of 9–17 μm and an initial length of 3–6 mm from Kamenny Vek Ltd. (Dubna, Russia). We used Grade H quality expanded graphene nanoparticles (GNP) from XG Sciences Inc. (Lansing, Michigan, USA) and NC3100 multi-walled CNTs from Nanocyl S.A. (Sambreville, Belgium) as nanosized particles. Graphene particles had an average thickness of 15 nm and an average diameter of 5–25 μm, as well as a specific surface area of 50–80 m^2/g. CNTs had an average diameter of 9.5 nm and an average length of 1.5 μm. The carbon purity of the nanotubes was above 95%.

2.2 | Sample preparation

We prepared the composites by continuous melt mixing using an LTE 26–44 twin-screw extruder ($L/D = 44$ and $D = 26$ mm) from Labtech Engineering Co., Ltd. (Thailand). The rotation speed of the extruder was 20 rpm, and the die temperature was 190°C. Before compounding, the PLA granulates were dried according to the recommendation of the producer (80°C, 4 h). We

15482634, 2024, 6, Downloaded from https://4spepublications.onlinelibrary.wiley.com/doi/10.1002/pen.26704, Wiley Online Library on [08/06/2024]. See the Terms and Conditions (https://onlinelibrary.wiley.com/terms-and-conditions) on Wiley Online Library for rules of use; OA articles are governed by the applicable Creative Commons License

prepared composites with a PLA matrix and basalt fiber (PLA + BF, 70–30 wt%) and hybrid composites with an additional 1 wt% nanoparticles (PLA + BF + CNT, PLA + BF + GNP). Nanocomposites were also prepared with 1 wt% nanoparticle content (PLA + CNT, PLA + GNP). In order to separate the effects of the reinforcing materials from the thermal effects, we extruded the PLA matrix. After the extrusion process, the product was granulated (particle size 4 mm) for further processing. Before the production of the injection-molded specimens, we dried the compounded materials again with the same parameters as before to avoid thermal degradation caused by the moisture content. The dumbbell-shaped specimens (with a cross-section of 4 mm × 10 mm, according to the ISO 527-2 standard) were injection molded on an Arburg Allrounder 370S 700–290 injection molding machine. Melt temperature was 190°C, and mold temperature was 25°C. The injection pressure used with the reference material and the nanocomposites was ∼1100 bar, and ∼1300–1550 bar for fiber-reinforced and hybrid composites.

For the investigation of the maximum damping capacity with the maximum crystalline ratio of the materials, we annealed some specimens for 2 h at 80°C. The parameters for anneling were chosen based on the results of Wang et al.,[29] as they achieved the highest crystalline fraction with these parameters.

2.3 | Characterization methods

We measured the melt flow index (MFI) with a Ceast 7027.000 plastometer (Instron Corporation, Massachusetts, USA) (210°C, 2.16 kg). We calculated the MFI values according to the ISO 1133-1:2011 standard.

Differential scanning calorimetry (DSC) was performed on a Q2000 DSC device (TA Instruments, USA) in an N_2 atmosphere (50 mL/min). The heating rate was 5°C/min, and a simple heat program was used in the temperature range of 0 to 200°C. The crystallinity of the materials was calculated with the following equations[30]:

$$X_1 = \frac{\Delta H_m - \Delta H_{cc}}{\Delta H_f * (1-\alpha)} * 100\,(\%), \quad (1)$$

$$X_2 = \frac{\Delta H_m}{\Delta H_f * (1-\alpha)} * 100\,(\%), \quad (2)$$

where ΔH_m is the measured heat of fusion, ΔH_{cc} is the heat of cold crystallization, and α (−) is the mass ratio of the additives. The heat of fusion of 100% crystalline PLA (ΔH_f) is 93.1 J/g.[10] Equation (1) determines the crystallinity of the materials produced (X_1), and Equation (2) shows potential maximum crystallinity (X_2).

The tensile tests were performed according to the EN ISO 527 standard on a Zwick Z005 (Zwick GmbH & Co. KG, Germany) universal testing machine. In the case of the reference PLA and the nanocomposites, the cross-head speed was 5 mm/min. In the case of the fiber-reinforced composites, it was 2 mm/min, due to the stiffness of these materials. Gauge length was 110 mm in all cases. We tested five specimens from each material produced.

After the tensile tests, the fracture surfaces were coated with a thin gold layer and analyzed by scanning electron microscopy (SEM) with a JEOL JSM-6380LA (JEOL Ltd., Japan) device.

Dynamic mechanical thermal analysis (DMA) was performed on a Q800 device from TA Instruments (USA) in dual cantilever mode with an amplitude of 15 μm and frequency of 1 Hz. The applied temperature range was 15–100°C, and the heating speed was 5°C/min.

3 | RESULTS AND DISCUSSION

3.1 | Melt flow index

In the case of a thermoplastic polymer composite melt, MFI can indicate how the presence of reinforcing materials and processing have affected viscosity.[23] The changes in viscosity can indicate the degradation of the PLA and the dispersion state of the nanomaterials. The degradation is illustrated by the fact that the MFI of the PLA in the data sheet published by the manufacturer is 14 g/10 min, while we measured 28.1 g/10 min after extrusion (Figure 1).

The MFI increased because PLA easily degrades by heat,[31] and we measured it after extrusion. During compounding, the material spent enough time in the extruder to start chain scission. Also, graphene slightly decreased

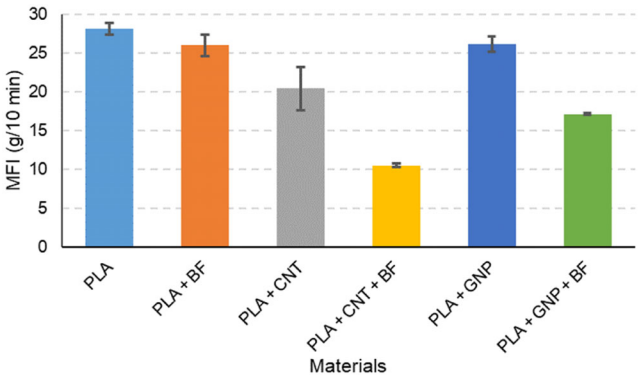

FIGURE 1 Melt flow index of the reference and the composite materials.

15482634, 2024, 6, Downloaded from https://4spepublications.onlinelibrary.wiley.com/doi/10.1002/pen.26704, Wiley Online Library on [08/06/2024]. See the Terms and Conditions (https://onlinelibrary.wiley.com/terms-and-conditions) on Wiley Online Library for rules of use; OA articles are governed by the applicable Creative Commons License

the material's ability to flow. For nanocomposites with CNTs, the MFI decreased more, so the material became more viscous due to the CNT, which indicates good dispersion. As expected, the MFI decreased slightly due to the basalt fibers. In hybrid composites, the decrease in the MFI and its smaller standard deviation shows that the basalt fibers helped distribute the nanoparticles properly. In the molten state of the PLA, the dispersed nanoparticles can efficiently hamper the movements of the molecules. When they are better dispersed, the nanoparticles bind to the matrix material over a larger area. Also, when nanotubes are used, the nanotubes and the molecules are also entangled with each other (Figure 2), resulting in a greater increase in viscosity for materials containing CNT.

3.2 | Tensile characteristics

The tensile curves of the nanocomposites (Figure 3) are similar to the curves of PLA, and the curves of the composites containing basalt fibers are very similar.

We determined the tensile strength, tensile modulus, and elongation at break of each material (Table 1).

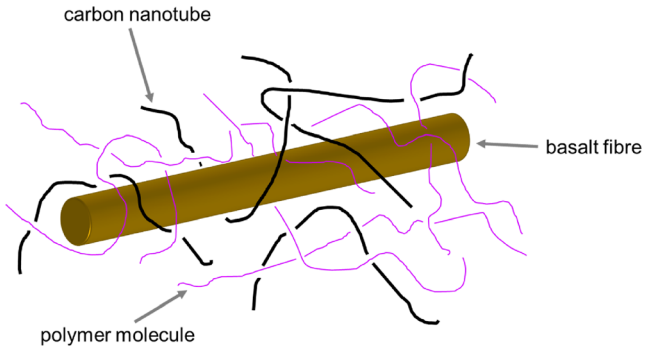

FIGURE 2 Imagined structure of poly(lactic acid) hybrid composites containing basalt fiber and carbon nanotubes.

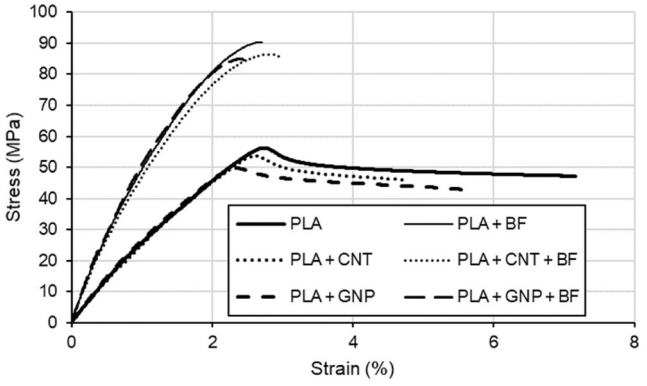

FIGURE 3 Strain–stress curves of the investigated materials.

Nanoparticles slightly decreased tensile strength but increased tensile modulus considerably. As will be shown later in the electron micrographs, aggregates of nanoparticles remained in the composites. The increased modulus indicates a good interaction between the nanoparticles and the matrix. Fracture in nanocomposites is not catastrophic; yield also occurs here, and failure was not triggered by the aggregates behaving as weak sites. This is probably because the molecules are bound to the surface of the nanoparticles, and so their movement is inhibited. Thus, they are not deformed to any great extent when tensile forces are applied. This means that the molecules further away from the nanoparticles take the deformation. This leads to lower yield stress.

Basalt fibers greatly improved tensile strength and tensile modulus. As expected, fiber reinforcement reduced elongation at break to less than half of that of the reference material. The nanocomposites increased tensile modulus, and the hybrid composite with graphene had a tensile modulus almost 400 MPa higher than that of the composite reinforced by basalt fibers only.

3.3 | Differential scanning calorimetry

The DSC analysis was necessary because we did not know the combined effect of the reinforcing materials on the morphology of the matrix previously. For us, the resulting crystalline ratio (X) and glass transition temperature (T_g) are important, as the former can have a significant influence on mechanical behavior and the latter indicates the application range.

The DSC curves (Figure 4) show that the reinforcing materials have only slightly altered the glass transition temperature of PLA. Due to the relatively fast cooling during injection molding, enthalpy relaxation occurred, which is especially prominent for hybrid composites. The large exothermic peaks of cold crystallization indicate that the materials only slightly crystallized after processing.

Tábi et al.[10] have performed a deep analysis of the thermal properties of semi-crystalline PLA, with particular emphasis on the α crystalline modification. Specifically, they investigated the effect of the ratio of the more stable α to the less stable α' modification on the thermomechanical and creep properties of the material. These two types of crystalline modifications of PLA are also visible in our cases: a less stable α' and a more stable α modification (first and second crystalline melting peaks, T_{m1} and T_{m2}, respectively). In the presence of graphene, the ratio of the less stable α' phase increased as the two crystalline melting peaks have nearly the same heights, while for the other materials, the second crystalline melting peak is larger. Also, in the composite containing GNP,

15482634, 2024, 6, Downloaded from https://4spepublications.onlinelibrary.wiley.com/doi/10.1002/pen.26704, Wiley Online Library on [08/06/2024]. See the Terms and Conditions (https://onlinelibrary.wiley.com/terms-and-conditions) on Wiley Online Library for rules of use; OA articles are governed by the applicable Creative Commons License

TABLE 1 Tensile properties of the composite materials.

Material	Tensile strength (MPa)	Tensile modulus (MPa)	Elongation at break (%)
PLA	56.5 ± 0.3	2797 ± 41	6.1 ± 1.3
PLA + BF	90.4 ± 1.1	6232 ± 96	2.7 ± 0.1
PLA + CNT	56.4 ± 0.7	2939 ± 23	5.3 ± 0.7
PLA + CNT + BF	87.1 ± 0.7	6177 ± 94	2.8 ± 1.1
PLA + GNP	49.6 ± 0.2	2975 ± 9	5.3 ± 0.6
PLA + GNP + BF	84.4 ± 0.4	6608 ± 90	2.4 ± 0.0

Abbreviations: BF, basalt fiber; CNT, carbon nanotube; GNP, graphene nanoparticles; PLA, poly(lactic acid).

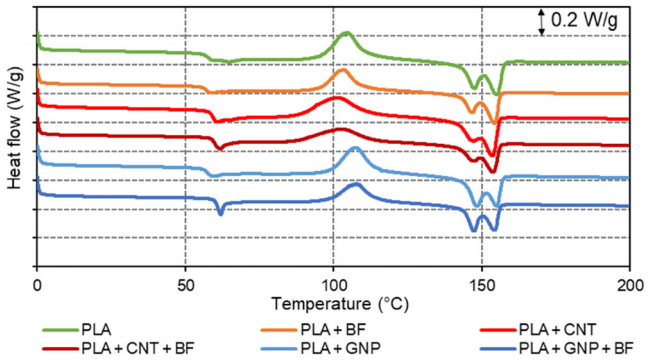

FIGURE 4 Heat flow of the materials (differential scanning calorimetry) after heating.

the basalt fiber did not help in creating more α crystallites; there is no difference between the nano- and the hybrid composite in this respect. However, CNT and basalt fibers sightly helped the creation of the more stable crystalline modification.

Table 2 presents the evaluated results of DSC, where T_g is the glass transition temperature, T_{cc} is the cold crystallization temperature, T_{m1} and T_{m2} are the melting temperatures of the α' and α crystalline modifications, respectively, X_1 and X_2 are the calculated crystalline ratios based on Equations (2) and (3).

Basalt fibers and graphene did not change T_g considerably. CNT, however, increased it. Hybrid composites show the highest values. Surprisingly, all this correlates well with the MFI and confirms the explanation we gave when we discussed MFI results. That is, nanoparticles reduce the mobility of the molecules when they are distributed well. CNT can be dispersed more easily than GNP, so it increased T_g even when used alone, but GNP only increased T_g when used in combination with basalt fibers.

The cold crystallization peaks varied depending on the nanoparticles used. One reason is that a change in the thermal conductivity affects the results. If it increases, the molecules in the total mass of the sample can become mobile enough to crystallize more quickly. The other reason is that the nanoparticles also hamper the movement of the molecules, as the molecules are bound to them by weak secondary bonds or can get entangled with the nanoparticles. This increases the energy required for crystallization, resulting in a shift of T_{cc} toward higher temperatures. Therefore, it is difficult to say what caused the changes. However, it seems that basalt fibers hardly changed T_{cc}, and nanoparticles were crucial in this respect: CNT decreased, and GNP increased T_{cc}, both in nano- and hybrid composites.

Previous research has already shown that the presence of nanotubes decreases the cold crystallization temperature and increases the ratio of more stable α crystallites.[32] Furthermore, it has been shown that in the case of graphene, the cold crystallization temperature

TABLE 2 Results of differential scanning calorimetry after heating.

Material	T_g (°C)	T_{cc} (°C)	T_{m1} (°C)	T_{m2} (°C)	X_1 (%)	X_2 (%)
PLA	57.6	104.6	147.4	155.1	0.8	28.7
PLA + BF	57.0	103.3	146.6	154.3	2.6	31.7
PLA + CNT	59.3	101.2	147.2	153.6	4.1	32.1
PLA + CNT + BF	59.7	102.6	147.7	153.6	2.6	33.2
PLA + GNP	57.4	107.6	148.4	155.1	2.3	28.3
PLA + GNP + BF	60.4	107.6	147.4	154.4	5.9	33.2

Abbreviations: BF, basalt fiber; CNT, carbon nanotube; GNP, graphene nanoparticles; PLA, poly(lactic acid).

15482634, 2024, 6, Downloaded from https://4spepublications.onlinelibrary.wiley.com/doi/10.1002/pen.26704, Wiley Online Library on [08/06/2024]. See the Terms and Conditions (https://onlinelibrary.wiley.com/terms-and-conditions) on Wiley Online Library for rules of use; OA articles are governed by the applicable Creative Commons License

increases, and the ratio of more stable α to less stable α' modification does not change significantly.[33] As a result of the present study, we have obtained similar results. One of the most probable explanations for these phenomena is that, in the case of nanotubes, the polymer molecules can loop through them. Thus, only a small fraction of the molecules adhere to the nanotube, so the remaining parts have sufficient mobility to crystallize. In addition, the good thermal conductivity of nanotubes allows a more uniform distribution of heat in the composite, so that the molecules start to thermally move at lower temperatures, which is reflected in lower T_{cc}. The sheet-like nature of graphene allows longer molecular parts to be attached to it, which means that molecules become mobile enough to crystallize at higher temperatures. Tábi et al.[10] annealed PLA at different temperatures. The DSC results suggest that the mobility of the molecules may be related to whether the more stable or less stable crystalline modification becomes dominant. In particular, the more stable α modification can be associated with the higher mobility. The presence of the basalt fiber had little effect on this phenomenon. In this respect, the impact of the nanoparticles is the decisive factor.

For applicability, the most important parameter is the crystalline ratio of the substance after processing and after slow cooling. All the reinforcements increased the crystalline ratio after processing, and graphene and basalt fiber together further increased it. The tendency is similar for the crystalline ratio at the end of the heating cycle—the crystalline ratio of the materials increased compared with neat PLA, and in the hybrid composites the additives produced a synergistic effect. PLA + GNP is an exception—it had similar crystallinity to neat PLA. We achieved the highest crystalline ratio in the PLA + GNP + BF hybrid material, with an almost 6% crystalline ratio after processing. This indicates the usefulness of hybridization.

3.4 | Dynamic mechanical thermal analysis

The DMA test is one of the most suitable methods to determine the dependence of mechanical properties on temperature, so we also examined the materials this way. It is clear from the curves (Figure 5) that the storage modulus of all composite materials increased compared with the reference PLA. It shows that more energy can be recovered from the composites after deformation than from PLA. We achieved remarkable results with the PLA + GNP + BF composite, whose storage modulus at room temperature is the highest of all the composites and nearly 2.5 times that of PLA.

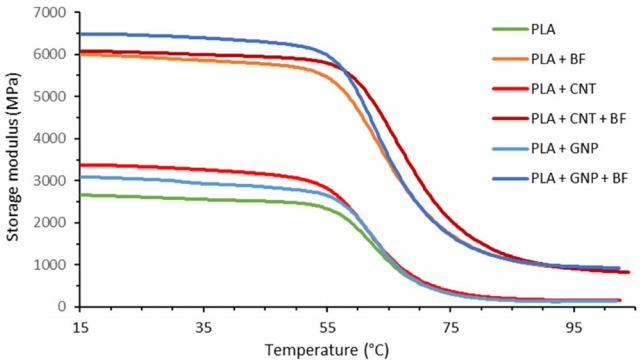

FIGURE 5 The storage modulus of each material.

Table 3 contains the evaluated results of DMA. The glass transition temperatures somewhat contradict the values obtained from the DSC curves—they are ∼5°C higher than those obtained by DSC, due to mechanical stress during measurement. Tan δ is related to the damping ability of a material. The tan δ_{max} values for composites containing only nanoparticles are not significantly different compared with PLA—segmental movements started for most of the molecules. This is because segmental movement was not activated in molecules bound to BF. It indicates a good interaction between the matrix and the reinforcing material, which was not changed by nanoparticles.

The storage modulus of nanocomposites and hybrid composites differs considerably. The nanoparticles increased the storage modulus below T_g (at 25°C) compared with PLA. Above T_g (80°C), the nanoparticles increased the storage modulus. The basalt fiber increased the storage modulus to more than 2.2 times of the neat PLA, and hybridization with nanoparticles resulted in improvement in each case below T_g.

3.5 | Scanning electron microscopy

We examined the fracture surfaces created during the tensile tests with a SEM. From the images, the failure process and fiber-matrix connection can be deduced, and the images show the distribution of particles in the matrix can be examined. In the case of the neat PLA (Figure 6A), the fracture surface is relatively flat, reflecting the relatively rigid behavior experienced during the tensile tests. The image of the basalt fiber–reinforced PLA (Figure 6B) shows that there was good adhesion. The fibers were well impregnated, and the cause of the failure was both fiber crack and fiber pullout. This explains the improvements in mechanical properties.

The PLA + CNT composite fracture surface also indicated rigid fracture (Figure 6C). In this case, at

15482634, 2024, 6, Downloaded from https://4spepublications.onlinelibrary.wiley.com/doi/10.1002/pen.26704, Wiley Online Library on [08/06/2024]. See the Terms and Conditions (https://onlinelibrary.wiley.com/terms-and-conditions) on Wiley Online Library for rules of use; OA articles are governed by the applicable Creative Commons License

TABLE 3 Results of DMA. E'_{25} is the storage modulus measured at 25°C, E'_{80} is the storage modulus measured at 80°C, T_g is the glass transition temperature at the inflection point of the storage modulus curve, tan δ_{25} is the tan δ measured at 25°C and tan δ_{max} is the maximum of the tan δ curve.

Material	E'_{25} (MPa)	E'_{80} (MPa)	T_g (°C)	tan δ_{25}	tan δ_{max}
PLA	2611	202	62.5	0.019	0.34
PLA + BF	5941	1332	63.3	0.017	0.20
PLA + CNT	3335	251	61.5	0.016	0.32
PLA + CNT + BF	6043	1513	65.7	0.019	0.20
PLA + GNP	3038	203	62.4	0.019	0.36
PLA + GNP + BF	6454	1320	62.8	0.016	0.22

Abbreviations: BF, basalt fiber; CNT, carbon nanotube; GNP, graphene nanoparticles; PLA, poly(lactic acid).

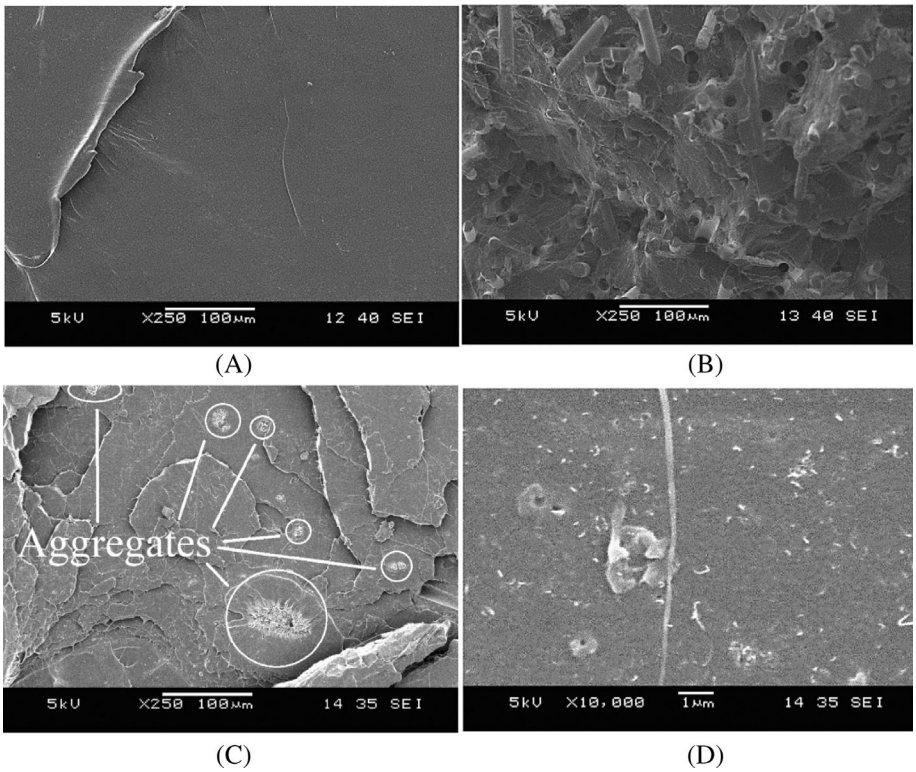

FIGURE 6 Fracture surface of (A) neat PLA and (B) PLA + BF at a magnification of 250× and the fracture surface of PLA + CNT at a magnification of (C) 250× and (D) 10,000×. BF, basalt fiber; CNT, carbon nanotube; PLA, poly(lactic acid).

very low magnification, nanotube aggregates can be noticed, which are present in large numbers, and some of them reached 100 µm in size. During the SEM examination, we did not find evidence that the crack started from one of the aggregates. Also, although there were some aggregates, the nanoparticles were well dispersed (Figure 6D).

When basalt fibers were added to the CNTs, the aggregates of the particles were completely eliminated, and the particles were successfully dispersed in the matrix (Figure 7). There was good adhesion between the matrix and the reinforcing materials. The matrix material was stuck to the surface of the pulled-out fibers; therefore, the impregnation of the reinforcing materials was adequate.

GNP is difficult to detect with SEM if it interacts well with the matrix. No GNP aggregates were detected at either low or high magnification, so, although they were likely to be in the composite based on its mechanical properties, they interacted with the matrix well (Figure 8A,B).

No GNP aggregates are visible on the fracture surfaces of the composites containing basalt fibers (Figure 8C,D). The characteristic size of individual GNPs is far smaller than that of CNTs, making them very difficult to detect by SEM. Also, PLA is highly susceptible to degradation during SEM examination, which prevents high-magnification images. Nevertheless, GNPs are also well dispersed in the hybrid composite, similarly to CNT + BF. At least, rheological, mechanical, and thermal properties and the absence of aggregates suggest this.

15482634, 2024, 6, Downloaded from https://4spepublications.onlinelibrary.wiley.com/doi/10.1002/pen.26704, Wiley Online Library on [08/06/2024]. See the Terms and Conditions (https://onlinelibrary.wiley.com/terms-and-conditions) on Wiley Online Library for rules of use; OA articles are governed by the applicable Creative Commons License

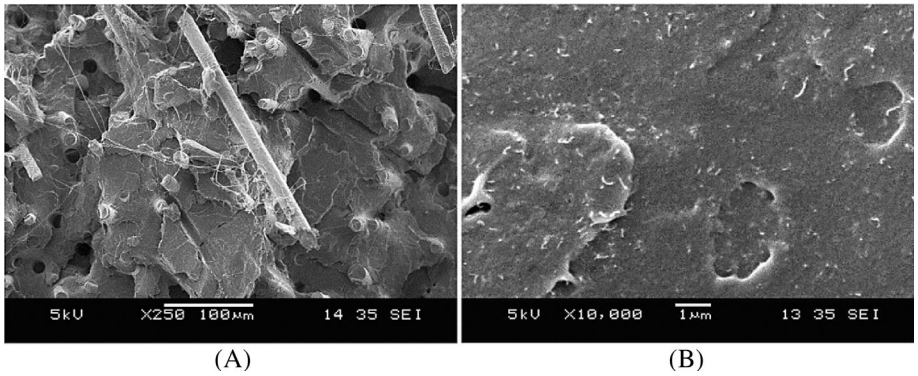

(A) (B)

FIGURE 7 Fracture surface of PLA + CNT + BF at a magnification of (A) 250× and (B) 10,000×. BF, basalt fiber; CNT, carbon nanotube; PLA, poly(lactic acid).

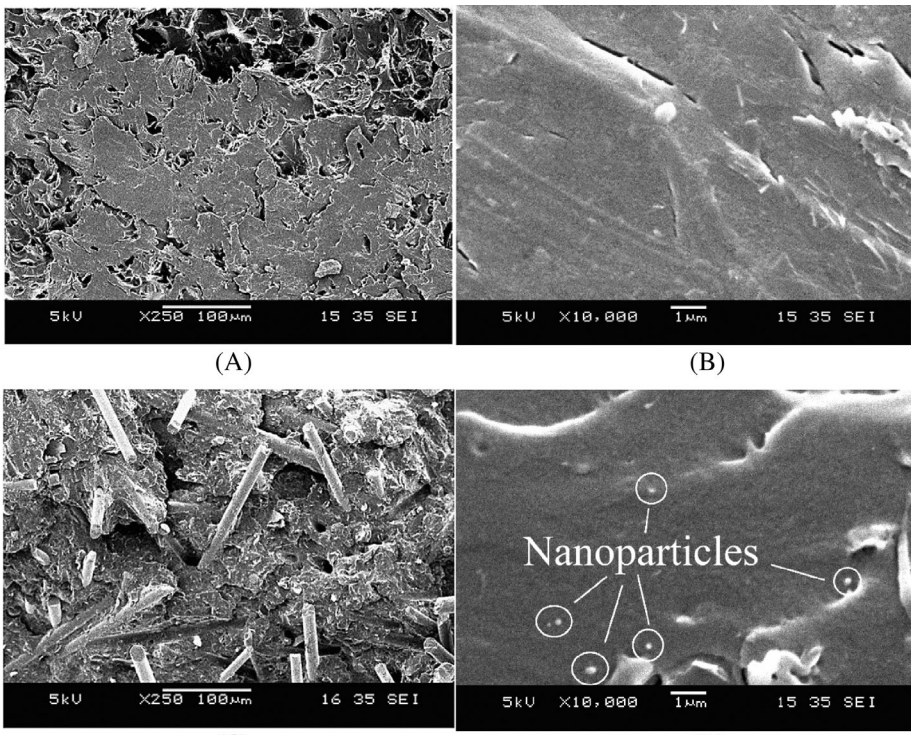

(A) (B)

(C) (D)

FIGURE 8 Fracture surface of PLA + GNP at a magnification of (A) 250× and (B) 10,000× and the fracture surface of PLA + GNP + BF at a magnification of (C) 250× and (D) 10,000×. BF, basalt fiber; GNP, graphene nanoparticles; PLA, poly(lactic acid).

4 | CONCLUSIONS

We prepared and investigated PLA composites containing basalt fiber and carbon-based nanoparticles (multi-walled CNTs and graphene). Basalt fibers increased strength significantly, which slightly decreased in hybrid composites. However, the hybrid composite containing graphene showed a significant improvement in tensile modulus. The DSC results showed that the crystalline ratio of the composites increased for all reinforcing materials. The most significant increase was measured for hybrids containing GNP. The increased modulus can, therefore, be partly explained by this. On the other hand, from the MFI results, we concluded that the improved nanoparticle distribution in the hybrid composites also contributed to the increased modulus. The glass transition temperature also increased in the hybrid composites, indicating good contact between the reinforcing materials and the matrix and a wider application temperature range. In the case of basalt fiber composites—including hybrid composites—the decrease in storage modulus at the glass transition temperature is less drastic than for other materials. This means that in some cases, composites can be used even above the glass transition temperature. SEM studies also confirmed that the dispersion of nanoparticles was better in hybrid composites than in nanocomposites. Overall, the hybrid composites showed favorable mechanical and thermal behavior, broadening the application of polylactic acid in engineering.

ACKNOWLEDGMENTS

Project no. TKP-6-6/PALY-2021 has been implemented with the support provided by the Ministry of Culture and Innovation of Hungary from the National Research,

15482634, 2024, 6, Downloaded from https://4spepublications.onlinelibrary.wiley.com/doi/10.1002/pen.26704, Wiley Online Library on [08/06/2024]. See the Terms and Conditions (https://onlinelibrary.wiley.com/terms-and-conditions) on Wiley Online Library for rules of use; OA articles are governed by the applicable Creative Commons License

Development and Innovation Fund, financed under the TKP2021-NVA funding scheme. László Mészáros is thankful for János Bolyai Research Scholarship of the Hungarian Academy of Sciences. The research was supported by the ÚNKP-23-5-BME-434 New National Excellence Program of the Ministry for Culture and Innovation from the source of the National Research, Development and Innovation Fund.

DATA AVAILABILITY STATEMENT

The data that support the findings of this study are available from the corresponding author upon reasonable request.

ORCID

László Mészáros https://orcid.org/0000-0001-5979-7403

REFERENCES

1. Avérous L. Biodegradable multiphase systems based on plasticized starch: a review. *J Macromol Sci Part C Polymer Rev*. 2004;44(3):231-274. doi:10.1081/MC-200029326
2. Cywar RM, Rorrer NA, Hoyt CB, Beckham GT, Chen EYX. Bio-based polymers with performance-advantaged properties. *Nat Rev Mater*. 2022;7(2):83-103. doi:10.1038/s41578-021-00363-3
3. RameshKumar S, Shaiju P, O'Connor KE. Bio-based and biodegradable polymers - state-of-the-art, challenges and emerging trends. *Curr Opin Green Sustain Chem*. 2020;21:75-81. doi:10.1016/j.cogsc.2019.12.005
4. Lendvai L, Omastova M, Patnaik A, Dogossy G, Singh T. Valorization of waste wood flour and Rice husk in poly(lactic acid)-based hybrid biocomposites. *J Polym Environ*. 2023;31(2):541-551. doi:10.1007/s10924-022-02633-9
5. Farah S, Anderson DG, Langer R. Physical and mechanical properties of PLA, and their functions in widespread applications—a comprehensive review. *Adv Drug Deliv Rev*. 2016;107:367-392. doi:10.1016/j.addr.2016.06.012
6. Tábi T, Pölöskei K. The effect of processing parameters and calcium-stearate on the ejection process of injection molded poly(lactic acid) products. *Period Polytech Mech*. 2022;66(1):17-25. doi:10.3311/PPme.18246
7. Haeldermans T, Samyn P, Cardinaels R, et al. Poly(lactic acid) bio-composites containing biochar particles: effects of fillers and plasticizer on crystallization and thermal properties. *Express Polym Lett*. 2021;15:343-360. doi:10.3144/expresspolymlett.2021.30
8. Lendvai L. Lignocellulosic agro-residue/polylactic acid (PLA) biocomposites: rapeseed straw as a sustainable filler. *Clean Mater*. 2023;9:100196. doi:10.1016/j.clema.2023.100196
9. Aliotta L, Vannozzi A, Cinelli P, Fiori S, Coltelli M-B, Lazzeri A. Wheat bran addition as potential alternative to control the plasticizer migration into PLA/PBSA blends. *J Mater Sci*. 2022;57(30):14511-14527. doi:10.1007/s10853-022-07534-9
10. Tábi T, Hajba S, Kovács JG. Effect of crystalline forms (α' and α) of poly(lactic acid) on its mechanical, thermo-mechanical, heat deflection temperature and creep properties. *Eur Polym J*. 2016;82:232-243. doi:10.1016/j.eurpolymj.2016.07.024
11. Zhang T, Wu H, Wang H, Sun A, Kan Z. Creation of fully degradable poly(lactic acid) composite by using biosourced poly(4-hydroxybutyrate) as bioderived toughening additives. *Express Polym Lett*. 2022;16:996-1010. doi:10.3144/expresspolymlett.2022.72
12. Virág ÁD, Tóth C, Molnár K. Photodegradation of polylactic acid: characterisation of glassy and melt behaviour as a function of molecular weight. *Int J Biol Macromol*. 2023;252:126336. doi:10.1016/j.ijbiomac.2023.126336
13. Zhang N, Zhao M, Liu G, Wang J, Chen Y, Zhang Z. Alkylated lignin with graft copolymerization for enhancing toughness of PLA. *J Mater Sci*. 2022;57(19):8687-8700. doi:10.1007/s10853-022-07101-2
14. Litauszki K, Petrény R, Haramia Z, Mészáros L. Combined effects of plasticizers and D-lactide content on the mechanical and morphological behavior of polylactic acid. *Heliyon*. 2023;9(4):e14674. doi:10.1016/j.heliyon.2023.e14674
15. Sadasivuni KK, Saha P, Adhikari J, Deshmukh K, Ahamed MB, Cabibihan J-J. Recent advances in mechanical properties of biopolymer composites: a review. *Polym Compos*. 2020;41(1):32-59. doi:10.1002/pc.25356
16. Tábi T, Égerházi AZ, Tamás P, Czigány T, Kovács JG. Investigation of injection moulded poly(lactic acid) reinforced with long basalt fibres. *Compos A: Appl Sci Manuf*. 2014;64:99-106. doi:10.1016/j.compositesa.2014.05.001
17. Khandelwal S, Rhee KY. Recent advances in basalt-fiber-reinforced composites: tailoring the fiber-matrix interface. *Compos Part B: Eng*. 2020;192:108011. doi:10.1016/j.compositesb.2020.108011
18. Vinay SS, Sanjay MR, Siengchin S, Venkatesh CV. Basalt fiber reinforced polymer composites filled with nano fillers: a short review. *Mater Today Proc*. 2022;52:2460-2466. doi:10.1016/j.matpr.2021.10.430
19. Ma P-C, Siddiqui NA, Marom G, Kim J-K. Dispersion and functionalization of carbon nanotubes for polymer-based nanocomposites: a review. *Compos Part A: Appl Sci Manuf*. 2010;41(10):1345-1367. doi:10.1016/j.compositesa.2010.07.003
20. Petrény R, Almásy L, Mészáros L. Investigation of the interphase structure in polyamide 6–matrix, multi-scale composites. *Compos Sci Technol*. 2022;225:109489. doi:10.1016/j.compscitech.2022.109489
21. Petrény R, Mészáros L. Moisture dependent tensile and creep behaviour of multi-wall carbon nanotube and carbon fibre reinforced, injection moulded polyamide 6 matrix multi-scale composites. *J Mater Res Technol*. 2022;16:689-699. doi:10.1016/j.jmrt.2021.12.030
22. Haghgoo M, Ansari R, Hassanzadeh-Aghdam MK. Prediction of electrical conductivity of carbon fiber-carbon nanotube-reinforced polymer hybrid composites. *Compos Part B: Eng*. 2019;167:728-735. doi:10.1016/j.compositesb.2019.03.046
23. Petrény R, Tóth C, Horváth A, Mészáros L. Development of electrically conductive hybrid composites with a poly(lactic acid) matrix, with enhanced toughness for injection molding, and material extrusion-based additive manufacturing. *Heliyon*. 2022;8(8):e10287. doi:10.1016/j.heliyon.2022.e10287
24. He H, Yang P, Duan Z, Wang Z, Liu Y. Reinforcing effect of hybrid nano-coating on mechanical properties of basalt fiber/poly(lactic acid) environmental composites. *Compos Sci Technol*. 2020;199:108372. doi:10.1016/j.compscitech.2020.108372
25. Zhu L, Qiu J, Liu W, Sakai E. Mechanical and thermal properties of rice straw/PLA modified by nano Attapulgite/PLA interfacial layer. *Compos Commun*. 2019;13:18-21. doi:10.1016/j.coco.2019.02.001

15482634, 2024, 6, Downloaded from https://4spepublications.onlinelibrary.wiley.com/doi/10.1002/pen.26704, Wiley Online Library on [08/06/2024]. See the Terms and Conditions (https://onlinelibrary.wiley.com/terms-and-conditions) on Wiley Online Library for rules of use; OA articles are governed by the applicable Creative Commons License

26. Lule Z, Kim J. Thermally conductive and highly rigid polylactic acid (PLA) hybrid composite filled with surface treated alumina/nano-sized aluminum nitride. *Compos Part A: Appl Sci Manuf*. 2019;124:105506. doi:10.1016/j.compositesa.2019.105506
27. Ramesh P, Prasad BD, Narayana KL. Influence of montmorillonite clay content on thermal, mechanical, water absorption and biodegradability properties of treated Kenaf fiber/ PLA-hybrid biocomposites. *Silicon*. 2021;13(1):109-118. doi:10.1007/s12633-020-00401-9
28. Ramesh P, Prasad BD, Narayana KL. Effect of MMT clay on mechanical, thermal and barrier properties of treated aloevera fiber/ PLA-hybrid biocomposites. *Silicon*. 2020;12(7):1751-1760. doi:10.1007/s12633-019-00275-6
29. Wang S, Daelemans L, Fiorio R, et al. Improving mechanical properties for extrusion-based additive manufacturing of poly(lactic acid) by annealing and blending with poly(3-hydroxybutyrate). *Polymers*. 2019;11(9):1529.
30. Lim LT, Auras R, Rubino M. Processing technologies for poly(lactic acid). *Prog Polym Sci*. 2008;33(8):820-852. doi:10.1016/j.progpolymsci.2008.05.004
31. Jaszkiewicz A, Bledzki AK, Duda A, Galeski A, Franciszczak P. Investigation of processability of chain-extended polylactides during melt processing – compounding conditions and polymer molecular structure. *Macromol Mater Eng*. 2014;299(3):307-318. doi:10.1002/mame.201300115
32. Kim SY, Shin KS, Lee SH, Kim KW, Youn JR. Unique crystallization behavior of multi-walled carbon nanotube filled poly(lactic acid). *Fibers Polymers*. 2010;11(7):1018-1023. doi:10.1007/s12221-010-1018-4
33. Wu D, Cheng Y, Feng S, Yao Z, Zhang M. Crystallization behavior of polylactide/graphene composites. *Ind Eng Chem Res*. 2013;52(20):6731-6739. doi:10.1021/ie4004199

How to cite this article: Juhász Z, Pinke B, Gonda B, Mészáros L. Effects of carbon-based nanoparticles on the properties of poly(lactic acid) hybrid composites containing basalt fibers and carbon-based nanoparticles processed by injection molding. *Polym Eng Sci*. 2024;64(6):2491-2500. doi:10.1002/pen.26704

15482634, 2024, 6, Downloaded from https://4spepublications.onlinelibrary.wiley.com/doi/10.1002/pen.26704, Wiley Online Library on [08/06/2024]. See the Terms and Conditions (https://onlinelibrary.wiley.com/terms-and-conditions) on Wiley Online Library for rules of use; OA articles are governed by the applicable Creative Commons License